COO-2166-24

A STUDY OF GRAIN BOUNDARY SEGREGATION

USING THE AUGER ELECTRON EMISSION TECHNIQUE

Annual Technical Progress Report - VII

D. F. Stein
L. A. Heldt
S. P. Clough
J. A. Hack
T. R. Pinchback
S. J. Vonk

Michigan Technological University
Department of Metallurgical Engineering
Houghton, Michigan 49931

January 1, 1977 - December 31, 1977

PREPARED FOR THE
U. S. ENERGY RESEARCH AND DEVELOPMENT ADMINISTRATION
UNDER CONTRACT NO. EY-76-S-02-2166.A001

rb

DISCLAIMER

ABSTRACT

An analysis of plastic flow at the tip of a propagating crack during brittle fracture has been developed in the course of this work. The plastic flow analysis takes into account the anisotropy of slip by a mixed mode opening scheme. Values of the true fracture energy for different crack systems are obtained; the effects of an embrittling agent can be taken into account.

The fracture stresses of Cu-Bi alloys having varied grain sizes and Bi concentrations were measured. Dilute alloys exhibited a decreasing fracture stress with decreasing grain size. Auger analysis indicated a large variation of Bi segregated to boundaries in coarse grained material with smaller variations in fine grained material.

The grain boundary diffusion of nickel was studied in the Cu-Bi alloy system by means of Auger spectroscopy. Bi retards boundary diffusion of Ni; however, the results are quite complex since the Ni presence alters the Bi concentration at the boundary. The Bi concentration tends to decrease to a value approximately equal to that of Ni.

Possible effects of solute segregation in determining SCC susceptibility of copper alloys in acid sulfate solution were examined with high purity binary alloys. Grain boundary segregation of Sb and Bi in Cu promoted intergranular SCC in sulfuric acid. Cracking was macroscopically brittle, but significant dissolution occurred along the intergranular crack path. Electrochemical measurements revealed an active path for SCC in segregated Cu-Sb and Cu-Bi alloys. Grain boundary segregation has no effect on the bulk electrochemical properties of unstressed Cu-Sb and Cu-Bi.

I. INTRODUCTION

The research program during the year 1977 has emphasized studies of brittle fracture, stress corrosion, and grain boundary diffusion processes as affected by segregation of solutes and impurities. This report summarizes results of the following specific research subjects:

A. Analysis of Plasticity at the Crack Tip During Intergranular Fracture

B. Effect of Grain Boundary Structure on Segregation

C. Effect of Grain Boundary Segregation on Grain Boundary Diffusion

D. Stress Corrosion of Copper Alloys Containing Segregated Solute Species

The experimental work has continued to have as a major thrust the direct measurement of the chemical composition of microstructural areas.

II. RESEARCH PROGRESS

A. Analysis of Plasticity at the Crack Tip During Intergranular Fracture

The substantial reduction in the fracture resistance of a grain boundary with impurity segregation is difficult to understand without considering the interrelation of true fracture stress and dislocation motion at the crack tip. It is well recognized that even in relatively brittle materials, the major portion of the energy of fracture is consumed by dislocation motion at the crack tip. Figure 1 provides a model to consider the interrelation between the true fracture stress and the dislocation motion. σ^* is defined as the stress necessary to part the atoms, σ_y is the yield stress, and σ_{nom} is the applied stress. When the stress at the crack tip exceeds the yield stress, plastic deformation occurs and when it exceeds the fracture stress, separation occurs. If one considers a crack approaching a volume element dV, its stress and strain history can

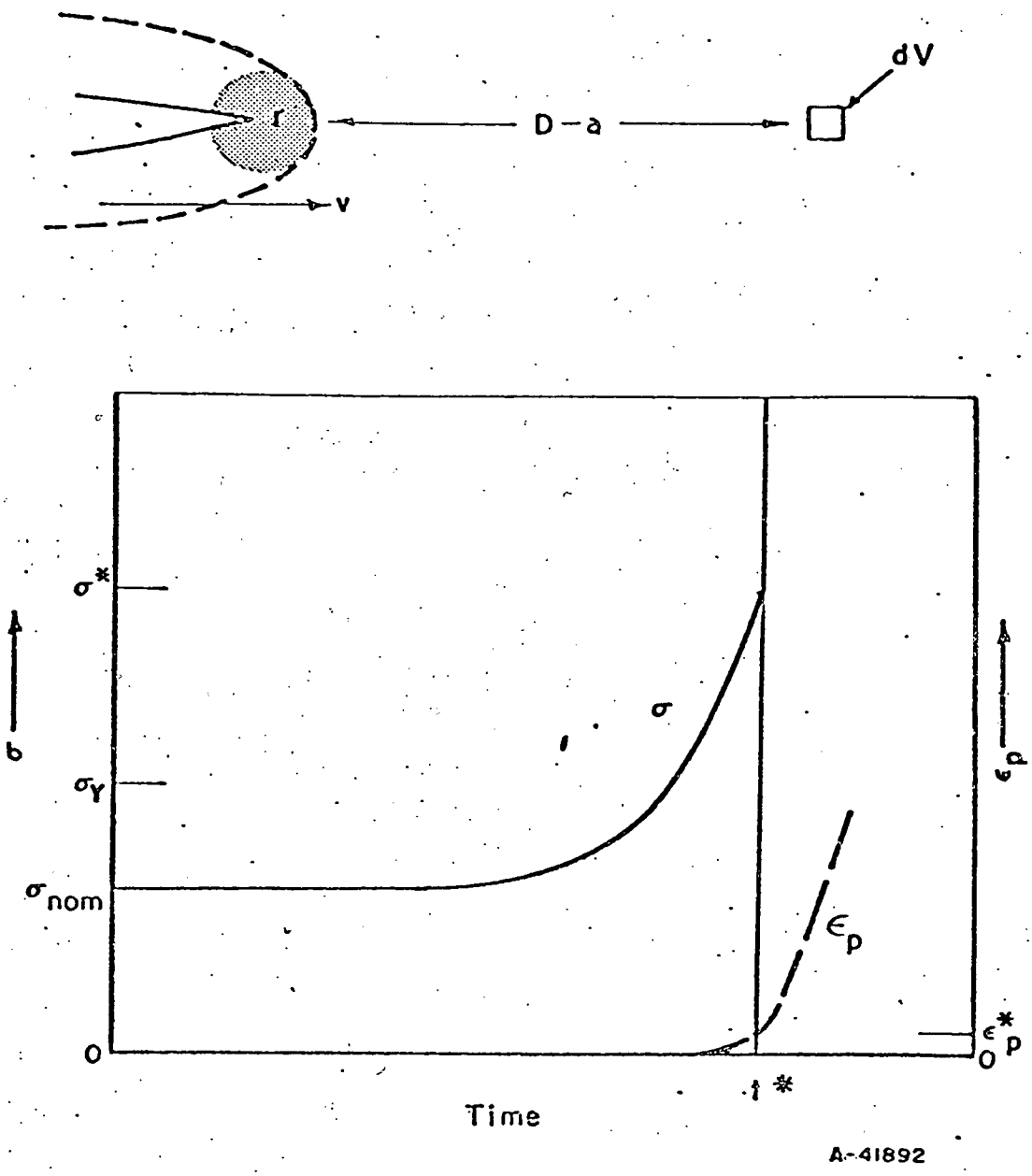

Figure 1 - Schematic representation of stress and plastic strain in a volume element dV ahead of a moving crack.

be described as shown in Figure 1. From dislocation measurements, it is observed that the dislocation velocity is a power function of stress represented by the empirical relation,

$$v = A\tau^m \tag{1}$$

where v = dislocation velocity

A = constant

τ = shear stress

m = dislocation velocity exponent.

Since m is between 10-40 for most engineering materials, a small increase in stress results in a major increase in dislocation velocity (plastic deformation). Therefore, a small decrease in the cohesive stress will result in a large decrease in the amount of plastic deformation.

Ayres and Stein (1) showed that the plastic deformation is anisotropic with respect to the plane on which fracture is occurring. For instance, they showed that the (100) fracture plane in bcc metals is preferred for cleavage even though the (110) plane usually has the lowest surface energy. This model has been extended by Hack and Stein to consider numerous planes and direction of fracture so that a close approximation to grain boundary fracture can be made. In the Hack and Stein model, the grain boundary is considered to be a series of very small cleavage planes.

Ayres and Stein (1) used the stress field of a superdislocation of Burger's vector Nb to represent that of a crack, after Friedel (2). A 1/r dependence of stress field derived from this model is only valid at distances far from the crack tip, i.e., at distances that are large in comparison to the dislocation spacing at the head of the pileup. A more appropriate stress field developed from linear elastic fracture mechanics for the region of the plastic zone exhibits a $\frac{1}{\sqrt{r}}$ dependence on position (3).

Therefore, this stress field was chosen for the calculation that follows and substituted into the calculation procedures developed by Ayres and Stein.

Figure 2 shows the calculated isovelocity contour at the tip of a crack for a tungstenlike material undergoing simple mode one crack opening. Given the dislocation velocity distribution ahead of the crack tip, the strain energy can be calculated if the stress time history is known.

1. Assumptions

The success of this model is ultimately limited by the ability to accurately describe the stress field and plastic flow in the plastic zone of a propagating crack. It has been assumed that the linear elastic solution for the stress field of a crack can be combined with Eq. 1, for the dislocation velocity to calculate the contours of constant dislocation velocity, Figure 2. This can be justified by the fact that the fracture mechanics stress fields only describe the stress state at the crack tip. Plasticity, or the deformation response of the material to the stress state, is governed by the dislocation dynamics expression of Eq. 1. The response of the dislocations to the stress field is assumed to be linear in the velocity ranges of 10^{-3}cm/sec to 10^{5} cm/sec on a log-log plot of dislocation velocity vs. stress. 10^{5} cm/sec is approximately the shear wave velocity in tungsten. Johnston and Gilman (4) have shown that, at dislocation velocities approaching the shear wave velocity in LiF, the velocity rises less sharply with the increasing stress than at low velocities. The dislocation velocity approaches the shear wave velocity asymptotically. Gilman (5) derived an exponential stress function that accurately predicted dislocation response in LiF, but Stein and Low (6) showed that the same type function did not work in Fe -3.25 Si. Since

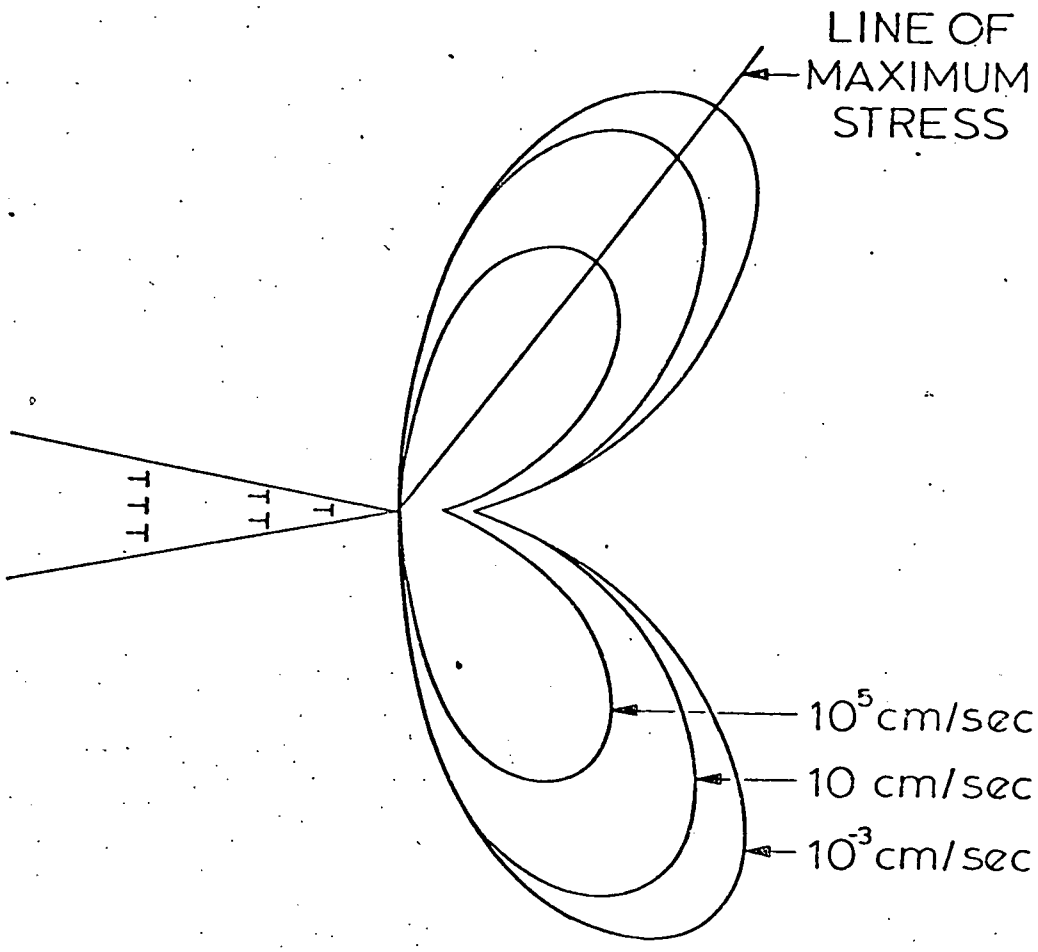

Figure 2 - Schematic of constant dislocation velocity contours ahead of a crack.

a satisfactory function has not been found for tungsten, the linear relationship will be assumed to hold.

Due to plastic relaxation of stresses at the crack tip, not all of the possible slip systems will actually be operative. To take this into account, only the slip system with the highest value of strain energy associated with it in each crack system will be assumed to be active. In addition, it will be assumed that in order for a volume element to yield, it will have to be stressed to at least the highest stress to which it has previously been exposed. This is a first approximation to account for work hardening. This assumption means that once the element has passed through the line of maximum stress in the plastic zone, as shown in Figure 2, yielding of the element stops.

Another limiting assumption is that the model inherently assumes that σ^* on all crystallographic planes is the same. Since the surface energy varies from plane to plane (Table I), this is obviously not the case. Until an accurate description of the dislocation velocity-stress response is obtained for high velocities, this situation cannot be handled. It should be realized that these assumptions are not as potentially damaging as they may seem. The real point of this work is to obtain relative values of true fracture energy (TFE) for different crack systems. The percentage differences between respective values of TFE will not be affected as much by the assumptions as by the absolute numbers.

2. Pure Mode I Opening Results

Two cases were considered: 1) a crack system which changes plane and front but not direction, and 2) a crack system which changes plane and direction but not crack front. Any other crack deflection can be described as a combination of these two cases. For both cases the

TABLE I. Surface Energy Functions

CRACK PLANE	ENERGY FUNCTION
{001}	$\frac{2\phi_1 + \phi_2}{d_o^2}$
{013}	$\frac{3\phi_1 + \phi_2}{\sqrt{5/2}\, d_o^2}$
{012}	$\frac{4\phi_1 + 3\phi_2}{\sqrt{5}\, d_o^2}$
{023}	$\frac{6\phi_1 + 5\phi_2}{\sqrt{13}\, d_o^2}$
{011}	$\frac{2(\phi_1 + \phi_2)}{d_o^2}$

(001)[100] crack system was considered the initial state. This agrees with the observations of Ayres (7). Calculations for Case 1 were made for (001)[100], (013)[100], (012)[100], (023)[100], and (011)[100] crack systems. Case 2 calculations were made for (001)[100], (103)[301], (102)[201], (203)[302], and (101)[101] crack systems. The results of the calculations are presented in Table II. ϕ_1 and ϕ_2 were obtained by solution of simultaneous equations using data generated from an averaging of Johnson and Morse potential functions for tungsten. All the pertinent material parameters, constants, functions and a copy of the computer program used can be found in Reference 8.

It can be seen from the TFE results for pure Mode I opening in Table II that the (001)[100] system has the lowest maximum value of strain energy by a large margin for Case 1 cracks. It should be noted that the strain energy fields were always symmetric with respect to the crack faces for the Case 1 cracks. It should also be noted that the strain energy fields of the crack systems which show lower strain energies than the (001)[100] system are not symmetric with respect to the crack faces. In addition, the strain energy values in the asymmetric systems deviate more and more from expectations as the angle between the crack plane and the (001) plane approaches 45°. All the calculated TFE values are well within the proper order of magnitude to be considered brittle fracture.

The key to understanding the discrepancy in the TFE values discussed above lies in the way in which a material would react to the assumed stress field. Calculations for high index crack systems show asymmetric slip responses with respect to the top and bottom faces of the crack. This means that different strain energies are associated with the opening of the top and bottom faces of the crack. Physically, this is impossible for a Mode I

TABLE II. Calculated Energy Results

Crack System	$2\gamma_s$ $(\frac{ergs}{cm^2})$	Pure Mode I Results		Mixed Mode Results	
		$\gamma_{p_{max}}$ $(\frac{ergs}{cm^2})$	TFE $(\frac{ergs}{cm^2})$	$\gamma_{p_{max}}$ $(\frac{ergs}{cm^2})$	TFE $(\frac{ergs}{cm^2})$
(001)[100]	7,560	6,314	12,794	6,314	12,794
(013)[100]	8,034	13,008	19,962	26,308	33,266
(012)[100]	7,980	15,396	22,296	28,508	35,408
(023)[100]	7,800	16,812	23,532	92,782	99,502
(011)[100]	7,270	17,910	24,100	536,006	542,196
(001)[100]	7,560	6,314	12,794	6,314	12,794
(103)[30$\bar{1}$]	8,034	5,228	12,182	17,070	24,024
(102)[20$\bar{1}$]	7,980	4,010	10,910	18,759	25,659
(203)[30$\bar{2}$]	7,800	2,051	8,771	27,913	34,633
(101)[10$\bar{1}$]	7,270	9,918	16,108	59,215	65,405

crack. Fracture of a material must provide two fresh surfaces. Given this restriction, the propagation of the high index crack systems cannot physically occur so the cracks would have to deflect. If the crack can deflect to any system under the influence of internal pressure, it will deflect to the one which requires the least energy for propagation. In this case, the crack will deflect to the (001)[100] system.

This argument can be carried further to crack systems which have symmetric stress fields but are not the minimum energy system. Even though the stress field is symmetric, there exists a tendency for an internally pressurized crack to move on the minimum energy system. The importance of these observations lies in the fact that if a crack is mathematically forced to propagate on a high energy plane in a high energy direction, so that the TFE of the crack system can be calculated, the opening mechanism of the crack cannot be considered to be pure Mode I as was previously thought. Pure Mode I opening can only occur on the minimum energy system. If a crack tries to deflect from the minimum energy plane or direction, shear must occur at the crack tip to force the crack open equally on the top and bottom surfaces. Shear at the crack tip induces Mode II and/or Mode III opening.

An attempt will be made to generalize the stress field equations to include mixed mode crack opening. Since the (001)[100] crack system is being considered the minimum energy system, it will always be in pure Mode I loading in an internally pressurized situation. Cracks on any other system must open in a mixed mode manner.

A mixed mode analysis requires the knowledge of the orientation of the crack plane, direction and front with respect to the axis of maximum normal stress. Since the (001)[100] system is assumed to be under the

influence of pure normal loading, the [001] direction will always be considered to be the tensile axis. The labeling of angles for a crack system of general orientation is given in Figure 3a. α is the angle between the crack front and the tensile axis, β is the angle between the crack propagation direction and the tensile axis, and γ is the angle between the crack plane normal and the tensile axis. For pure Mode I loading, $\alpha = \beta = 90°$. In the angular scheme of Figure 3a, Case 1 cracks are represented in Figure 3b as mixed Mode I-Mode III cracks. Case 2 cracks are shown in Figure 3c as mixed Mode I-Mode III cracks. Any crack system with a high indices plane, propagation direction and front would open under mixed Mode I-Mode II-Mode III conditions.

A general stress field equation for mixed mode opening is required for the proper calculation of the strain energies associated with the high energy systems. This can be derived from basic linear elastic fracture mechanics theory. Equation 2 gives the general relationship for K_{IC} (23):

$$K_{IC} = \sigma_{Fi}\sqrt{\pi a} \tag{2}$$

for a crack in an infinite body where:

K_{IC} = critical stress intensity factor for Mode I

σ_{Fi} = fracture stress in Mode I

a = half crack length.

The area of the general crack plane shown in Figure 3a is given by:

$$\frac{A}{\cos(\frac{\pi}{2} - \beta)\cos(\frac{\pi}{2} - \alpha)} = \frac{A}{\sin\beta\sin\alpha} \tag{3}$$

where A = area of a plane perpendicular to the tensile axis.

Combining Eqs. 2 and 3 and remembering that stress is load divided by area yields:

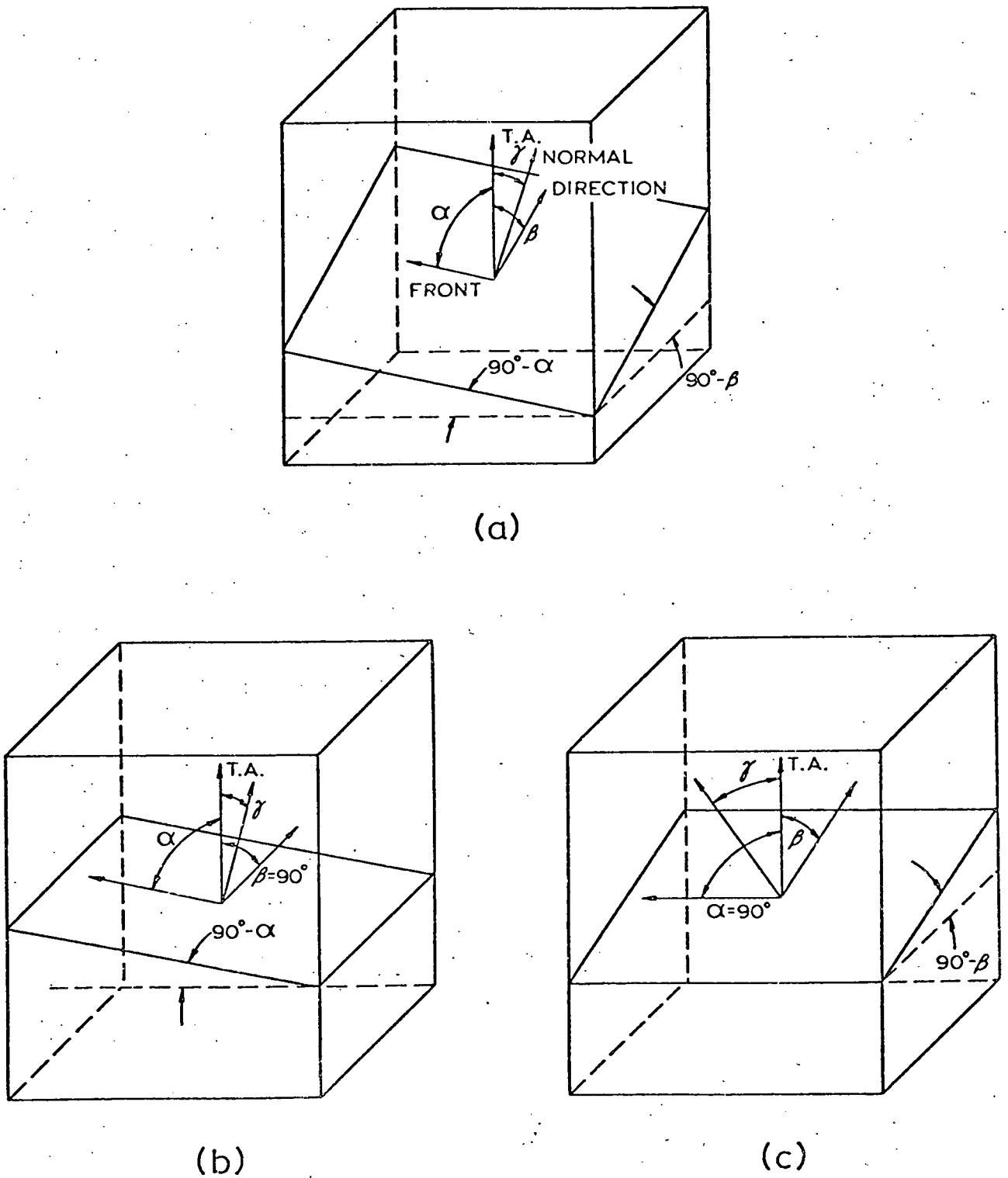

Figure 3 - General axes orientations for a general crack plane: a) Mixed Mode I, Mode II, Mode III; b) Mixed Mode I, Mode III; c) Mixed Mode I, Mode II

$$K_I = \cos\gamma\sin\alpha\sin\beta\sigma \text{ applied } \sqrt{\pi a}$$

$$K_{II} = \cos\beta\sin\alpha\sin\beta\sigma \text{ applied } \sqrt{\pi a} \qquad (4)$$

$$K_{III} = \cos\alpha\sin\alpha\sin\beta\sigma \text{ applied } \sqrt{\pi a} \ .$$

By manipulation of Eqs. 4, K_{IIC} and K_{IIIC} can be expressed in terms of K_{IC} as:

$$K_{IIC} = \left(\frac{\cos\beta}{\cos\gamma}\right) K_{IC}$$

$$K_{IIIC} = \left(\frac{\cos\alpha}{\cos\gamma}\right) K_{IC}. \qquad (5)$$

Thus, the stress field equations can be expressed in terms of the easily determined Mode I critical stress intensity factor. A combination of Eqs. 5 and Sneddon's expressions for Mode I, Mode II and Mode III stress fields (9) gives the stress equations for general mixed mode as:

$$\sigma_{xx} = \frac{K_{IC}}{\sqrt{2\pi r}}\left[\cos\frac{\theta}{2}\left(1-\sin\frac{\theta}{2}\sin\frac{3\theta}{2}\right) - \left(\frac{\cos\beta}{\cos\gamma}\right)\sin\frac{\theta}{2}\left(2+\cos\frac{\theta}{2}\cos\frac{3\theta}{2}\right)\right]$$

$$\sigma_{yy} = \frac{K_{IC}}{\sqrt{2\pi r}}\left[\cos\frac{\theta}{2}\left(1+\sin\frac{\theta}{2}\sin\frac{3\theta}{2}\right) + \left(\frac{\cos\beta}{\cos\gamma}\right)\sin\frac{\theta}{2}\cos\frac{\theta}{2}\cos\frac{3\theta}{2}\right]$$

$$\sigma_{zz} = \nu(\sigma_{xx}+\sigma_{yy}) = \frac{2\nu K_{IC}}{\sqrt{2\pi r}}\left[\cos\frac{\theta}{2} - \left(\frac{\cos\beta}{\cos\gamma}\right)\sin\frac{\theta}{2}\right] \qquad (6)$$

$$\tau_{xy} = \frac{K_{IC}}{\sqrt{2\pi r}}\left[\sin\frac{\theta}{2}\cos\frac{\theta}{2}\cos\frac{3\theta}{2} + \left(\frac{\cos\beta}{\cos\gamma}\right)\cos\frac{\theta}{2}\left(1-\sin\frac{\theta}{2}\sin\frac{3\theta}{2}\right)\right]$$

$$\tau_{xz} = \frac{K_{IC}}{\sqrt{2\pi r}}\left(\frac{\cos\alpha}{\cos\gamma}\right)\sin\frac{\theta}{2}$$

$$\tau_{yz} = \frac{K_{IC}}{\sqrt{2\pi r}}\left(\frac{\cos\alpha}{\cos\gamma}\right)\cos\frac{\theta}{2}.$$

If α, β, and γ are referred to the minimum energy crack plane, normal Eqs. 6 give the general stress field imposed by internal pressure on a crack system in a material which exhibits asymmetric slip response.

3. Mixed Mode Results

The plastic strain energies and TFE values for the Case 1 and Case 2 cracks were recalculated using the generalized stress field of Eq. 6. These results are also given Table II. The results give generally higher values of TFE than in the pure Mode I case. This would be expected from the additional stress field components. In addition, the (001)[100] crack system is now the minimum energy system in all cases. This, of course, does not conclusively prove that the present interpretation is correct, but it is extremely encouraging. The (011)[100] and (101)[101] again show the maximum TFE values in their respective groups.

The data of Table II shows that the TFE of a {110} crack would have to be reduced by about 80% in order for a crack to move off an {001} crack system onto a {110} system. Therefore, a substantial amount of reduction in plastic strain to fracture must occur for a crack to leave the cleavage mode and follow a grain boundary in tungsten. This can be accomplished by a relatively small decrease in σ^*, the theoretical fracture stress, which can be brought about by segregation of impurities to the grain boundaries. Also, a decrease in temperature, insterstitial hardening by impurities or anything else which contributes to slip constraint will tend to decrease the plastic strain to fracture.

4. Conclusions

1) The proposed model does not agree with experimental observations if pure Mode I opening is assumed for an internally pressurized crack. If anisotropy of slip is taken into account by a mixed mode opening scheme, the model appears to predict TFEs in the proper ranges.

2) The data generated in this study can now be used to obtain percentage estimates of the effect of an embrittling agent on σ^*

in tungsten vs. composition. Phosphorous would be a particularly interesting case due to its severe embrittling effect on tungsten.

3) The model can be generalized even further to include externally applied stresses and anisotropic elasticity so that other applications and materials may be studied.

B. Effect of Grain Boundary Structure on Segregation

Grain size has been known to have an effect on brittle fracture. In general, the finer the grain size the more ductile the material. For cleavage fracture, this is explained on the basis of free slip length which will relate to the maximum stress concentration to be developed at the intersection of a slip band with a grain boundary. For the case of grain boundary fracture, the explanation could be either that the fine grained material depletes the matrix of impurities because of the greater grain boundary surface (S) to total volume (V) ratio or because of the stress concentration argument used for cleavage fracture. To separate these two possibilities, alloys of Cu-Bi (Table III) of differing grain size and Bi concentration were prepared, their fracture stress determined, and the grain boundary fractures analyzed by Auger electron spectroscopy (AES). The relation between the S/V ratio and the fracture stress are shown in Figure 4.

The results are surprising. The dilute alloys show a decreasing fracture stress with decreasing grain size (an increasing S/V ratio) and the 180 ppm Bi alloy shows only a small increase in fracture stress with decreasing grain size. The behavior is consistent with expectations and previous work (Figure 5) with regard to the effect of bulk concentration on fracture stress. However, AES analysis showed a wide variation (Figure 6) in Bi segregated to grain boundaries in the coarse grain materials,

Table III. Alloy Compositions Used in This Study

Alloy Designation	Alloy Composition		
	Bi	O_2	Cu
I	40 wt. ppm	5 wt. ppm	Balance
II	150 wt. ppm	3 wt. ppm	Balance
III	180 wt. ppm	3 wt. ppm	Balance

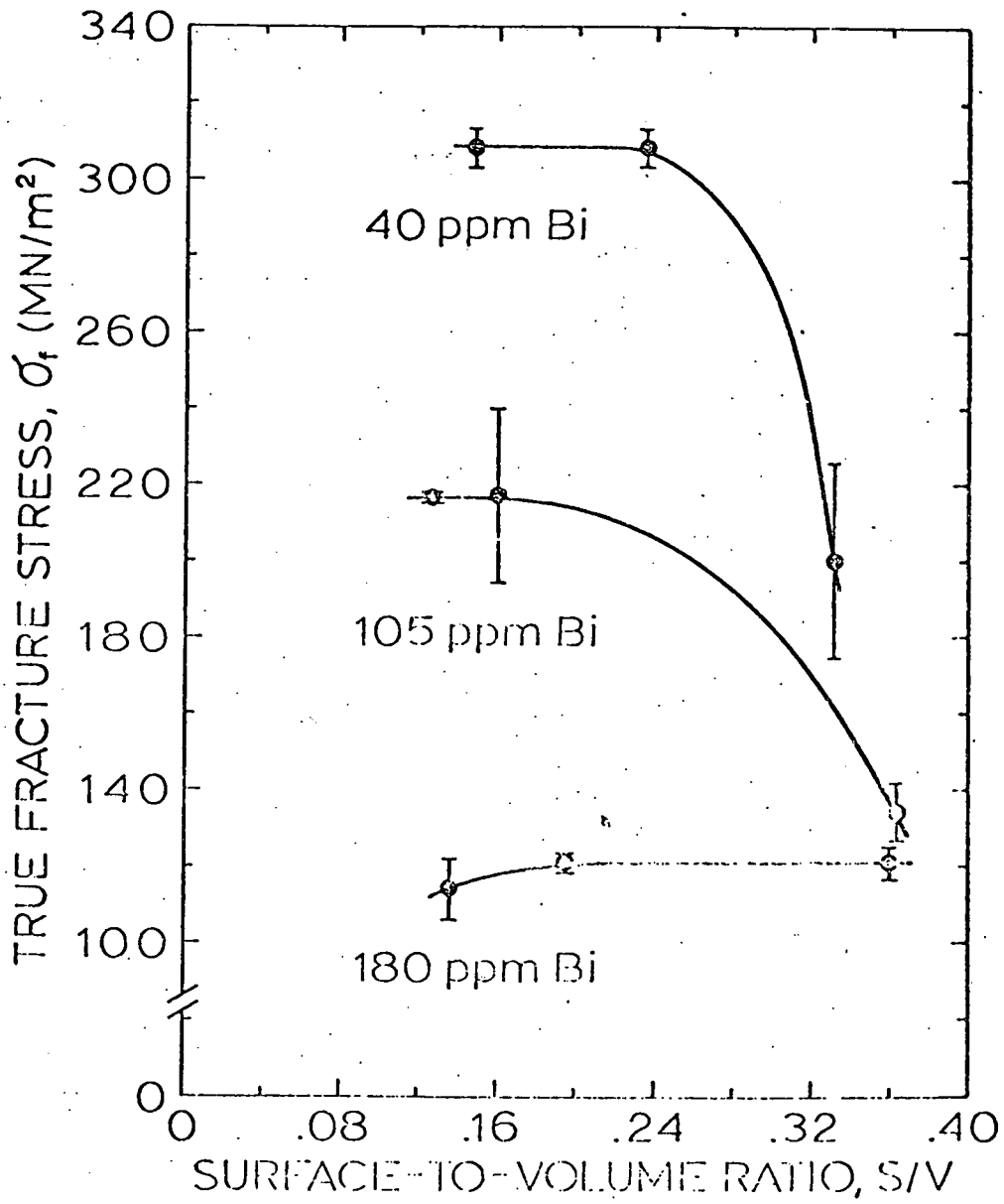

Figure 4. True fracture stress as a function of surface-to-volume ratio.

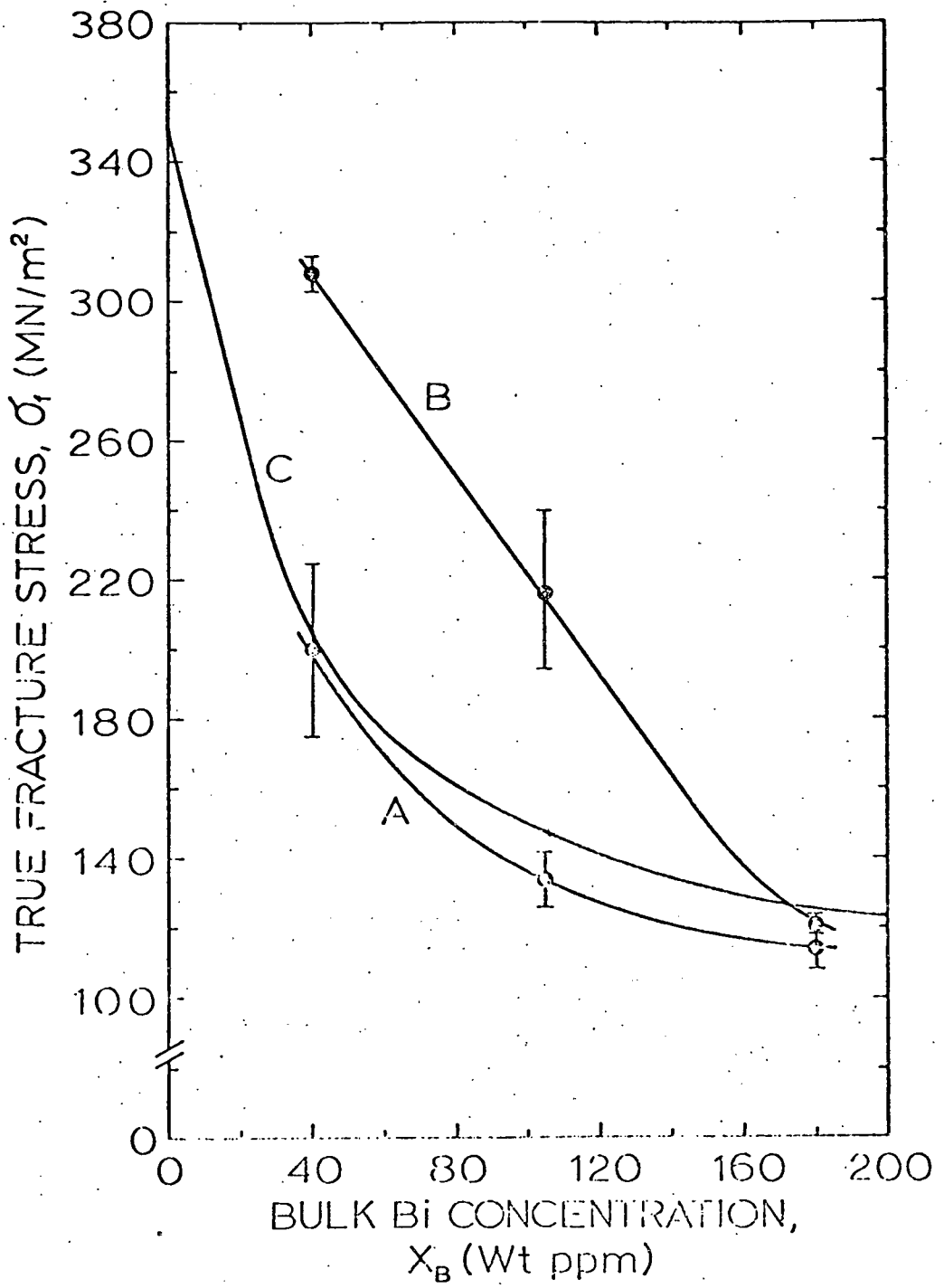

Figure 5. True fracture stress as related to bulk Bi concentration. Curve A: fine grained specimens; Curve B: intermediate and course grained specimens; Curve C: from Hondros and McLean (48).

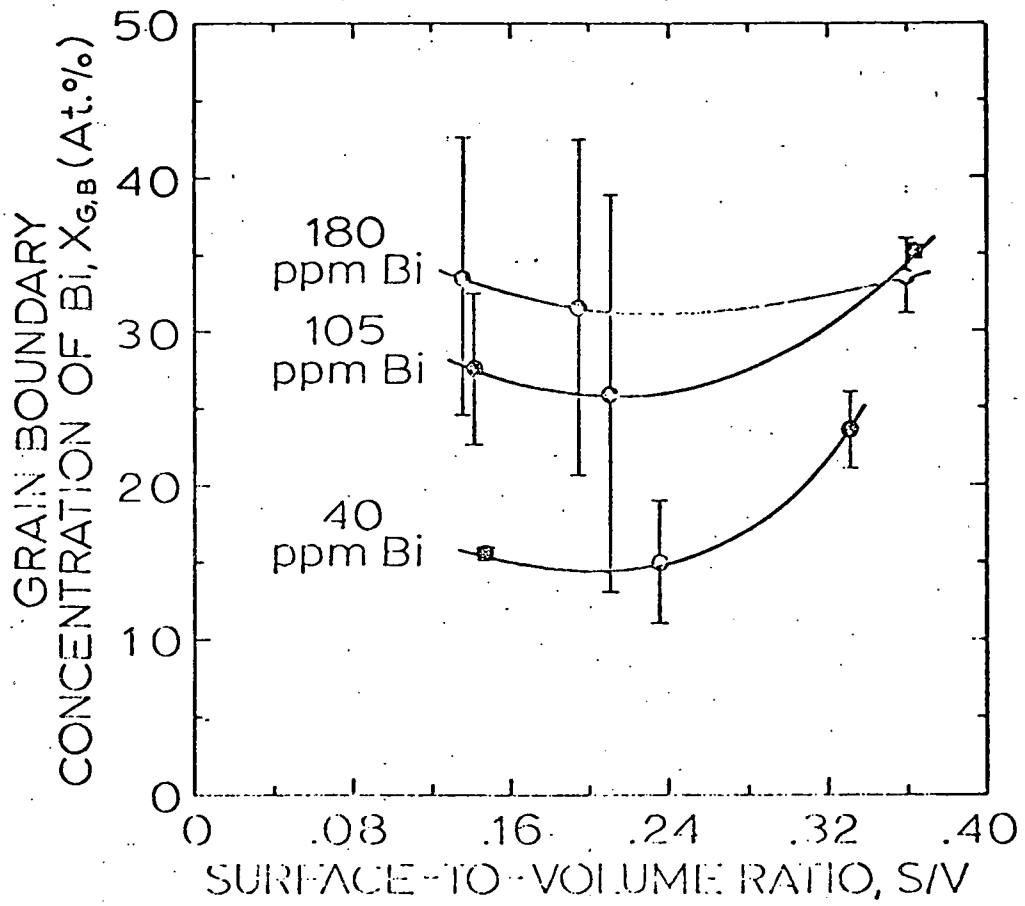

Figure 6. AES results as related to the surface-to-volume ratio.

with a smaller variation in the fine grained. The dilute alloy (40 ppm Bi) showed a substantial increase in Bi concentration at the grain boundaries in the fine grain size condition. The higher concentration Bi alloys showed certain grain facets in the coarse grain size that had substantially less Bi segregated than the fine grained materials. Since the fracture behavior will be controlled by the least embrittled boundary that fractures, it is not surprising, once the chemical composition of the grain boundary region is known, that the coarse grained materials had a higher fracture stress.

The increased segregation measured in the finer grained materials may be a consequence of the procedures used to prepare the materials. Table IV gives the cold work and heat treat schedule and grain growth annealing schedule as shown in Table V. The finer grain size materials will, on the average, have grain boundaries of higher energy since the annealing has not proceeded as far. If this is true, one would expect greater segregation at these grain boundaries since a major source of energy for grain boundary segregation is grain boundary energy. This would be consistent with the increased concentration of Bi measured in the fine grained materials. It was also observed that the variation in Bi concentration is not as great in the fine grained materials. The ease of fracture is related to the availability of an easy fracture path. While the small grain size results in a greater amount of surface area created upon fracture, it also permits a number of alternative fracture paths for the material. As shown schematically in Figure 7, the fracture path in the large grain size alloys is dictated by the few boundaries which are orientated in the proper way to allow sufficient resolved normal stress to cause boundary separation. The finer grained material, on the

Table IV. Specimen Cold Work and Heat Treatment Schedule

1.	Vacuum cast
2.	Solution anneal: 800°C - 2 hrs., H_2O quench
3.	Cold work (by swaging): 56% R.A.
4.	Solution anneal: 800°C - 2 hrs., H_2O quench
5.	Cold work: 44% R.A.
6.	Solution anneal: 800°C - 2 hrs., H_2O quench
7.	Cold work: 44% R.A.
8.	Solution anneal: 800°C - 2 hrs., H_2O quench
9.	Cold work: 75% R.A.
10.	Specimens machined at this time
11.	Recrystallization and grain growth anneal: 800°C, H_2O quench
12.	Segregation anneal: 527°C - 2 hrs.,* H_2O quench

* Some samples were segregated for longer times in order to ascertain the proper equilibrium segregation time for the low Bi, small grain size alloy.

Table V. Grain Growth Annealing Schedule

Alloy	Grain Growth Annealing Time (min.)
I	2.0
	30.0
	360.0
II	2.0
	15.0
	120.0
III	2.0
	15.0
	120.0

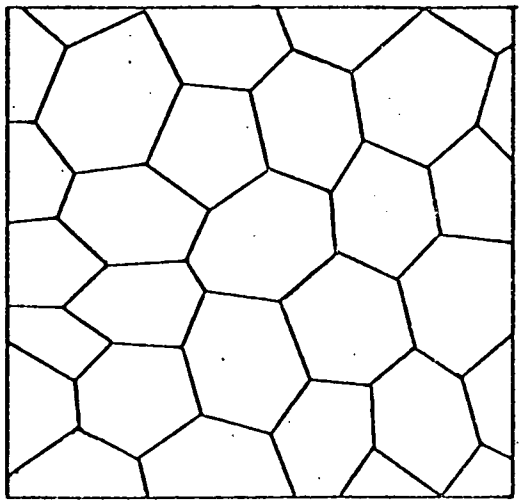

(A)

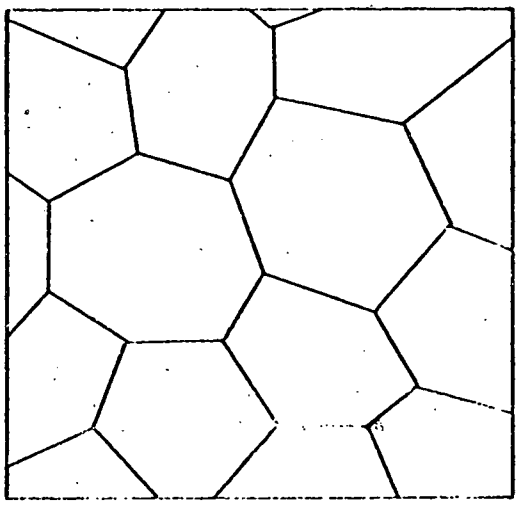

(B)

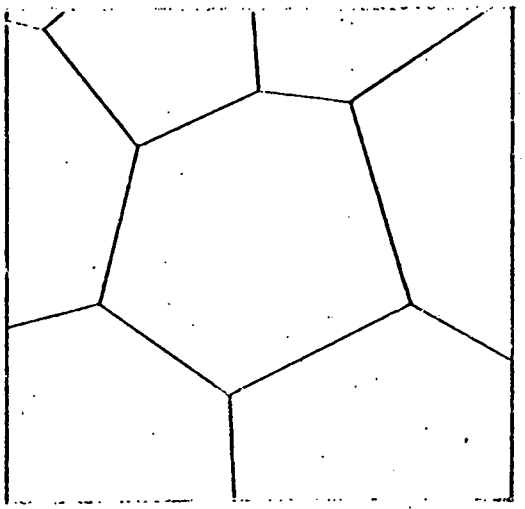

(C)

Figure 7. Schematic representation of grains and grain boundary fracture paths for three grain sizes.

other hand, will have many more paths available, many of which will be along the heavily segregated boundaries.

This study has shown that segregation to grain boundaries is highly variable and therefore, grain boundary orientation probably does play an important role in segregation. The effect was most pronounced in the coarse grained materials, but the smaller variation in the fine grained material is probably due to alternative fracture paths selecting the most highly segregated boundaries.

The grain size effect on fracture stress was a surprise, but after the Bi concentration was determined by AES, it was easily explainable. It is clear that the grain boundary fracture is primarily controlled by grain boundary chemical composition and not by the free slip length between grain boundaries. With equivalent segregation, the fine grained materials were no stronger than the coarse grained materials.

C. Effect of Grain Boundary Segregation on Grain Boundary Diffusion

Diffusion along grain boundaries is an important method of material transport at low temperatures because the activation energy for grain boundary diffusion is usually about 1/2 that for bulk diffusion. In recent years, it has become important technologically because thin film devices that carry high currents fail because of electrotransport along grain boundaries. In aluminum thin film conductors, it was found that trace amounts of copper had a very beneficial effect and this was attributed to the segregation of copper to the aluminum grain boundaries, filling the open spaces in the boundary and therefore raising the activation energy for grain boundary diffusion.

The Cu-Bi system was chosen to study grain boundary diffusion of nickel. The Cu-Bi could be made to fracture along grain boundaries and

the nickel Auger signal was easily detectable in the Cu-Bi matrix. It was expected that the Bi would retard the migration of Ni along the grain boundaries, and it was hoped that information on the activation energy for grain boundary diffusion of nickel with Bi segregation would provide a basis for understanding in a quantitative way the effect of segregation on grain boundary diffusion. Qualitatively, one would expect that when the open sites (about 33% of the grain boundary volume) were filled, the activation energy for grain boundary diffusion of nickel would be about the same as for bulk diffusion. It was found that Bi segregation did retard grain boundary diffusion of Ni, but the results were much more complicated than expected.

Figures 8 and 9 show the measured concentration of Bi and Ni at a copper fracture surface after various annealing times. The nickel had been plated on the surface and the annealing temperature was 530°C. It is observed that the Bi desegregates from the grain boundary as the Ni penetrates until about equal amounts of Ni and Bi are attained. Comparison of Figures 8 and 9 also shows that the greater concentration of Bi in the 180 ppm Bi alloy has a significant effect on the rate of penetration of Ni. Figures 10-12 show results on a Cu-60 ppm Bi alloy with various amounts of iron (Fe additions reduce Bi segregation). The results again show the Bi retarding nickel penetration and the reduction in Bi concentration at the grain boundaries until it reaches an equal level with the nickel. The following statements generalize the experimental results:

1. The lower the effective Bi concentration in the alloy, the greater the Ni penetration for any given diffusion time.

2. The longer the time for diffusion, the greater the Ni penetration in a given alloy.

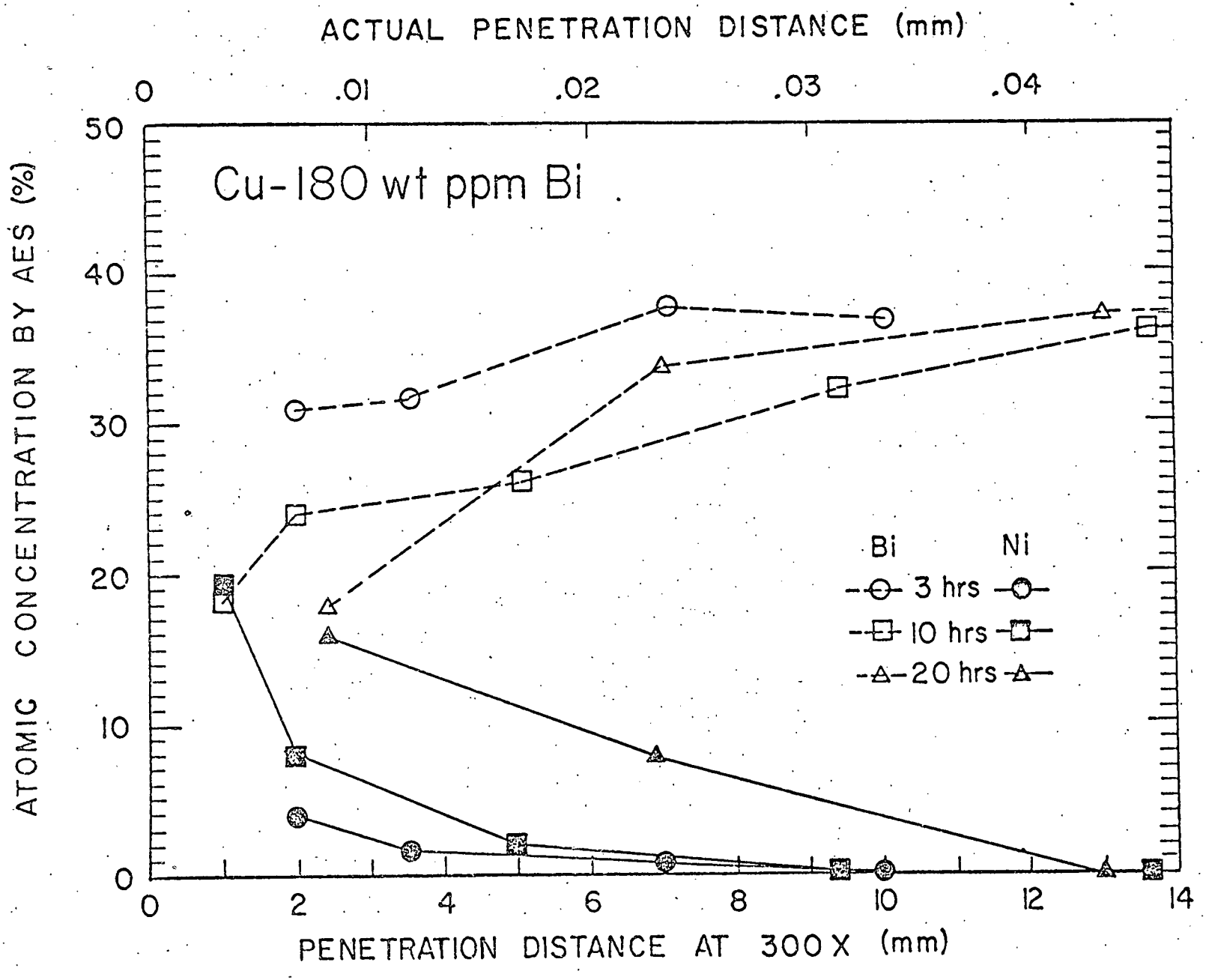

Figure 8. Atomic concentration versus penetration distance, Cu-180 wt ppm Bi.

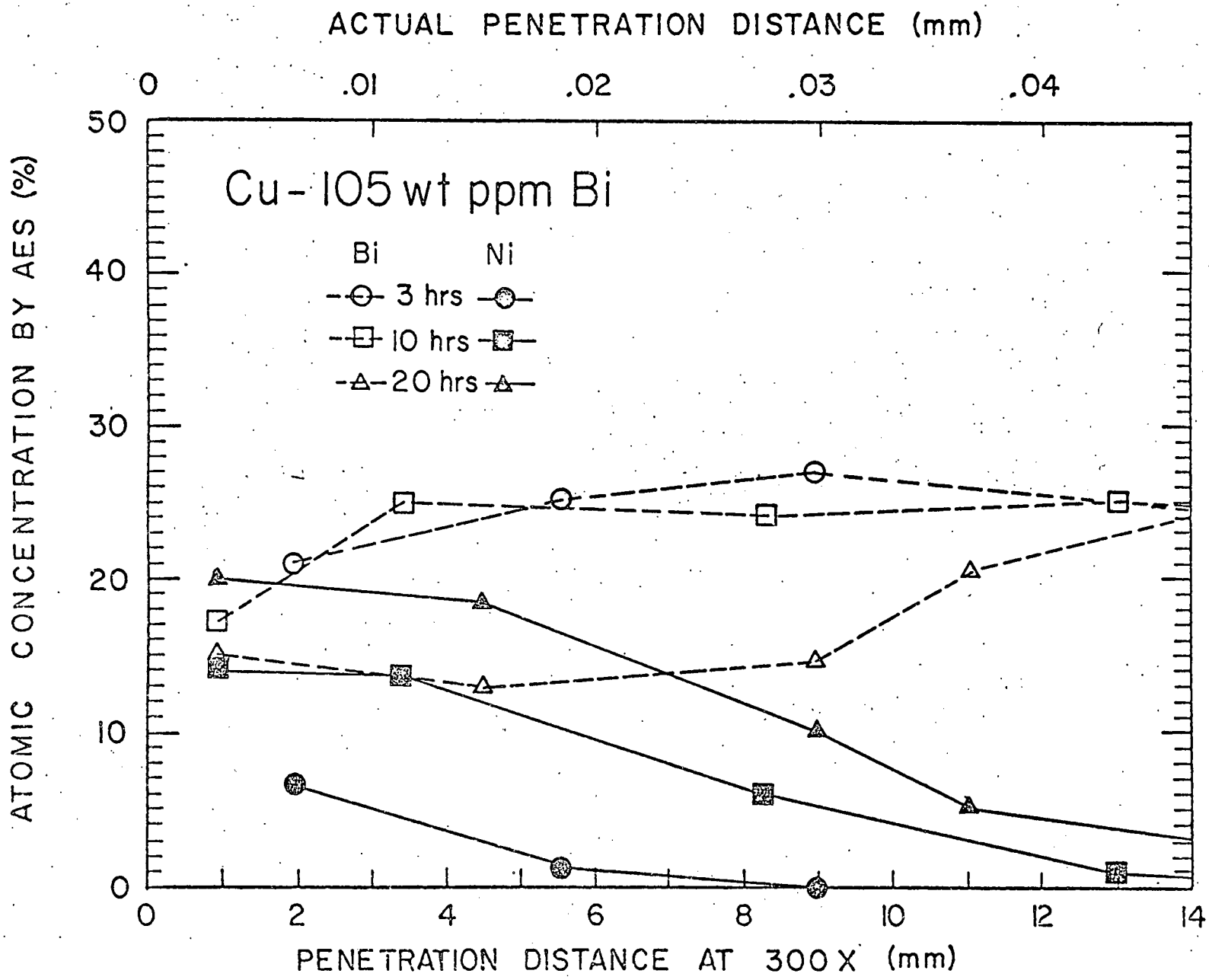

Figure 9. Atomic concentration versus penetration distance, Cu-105 wt ppm Bi.

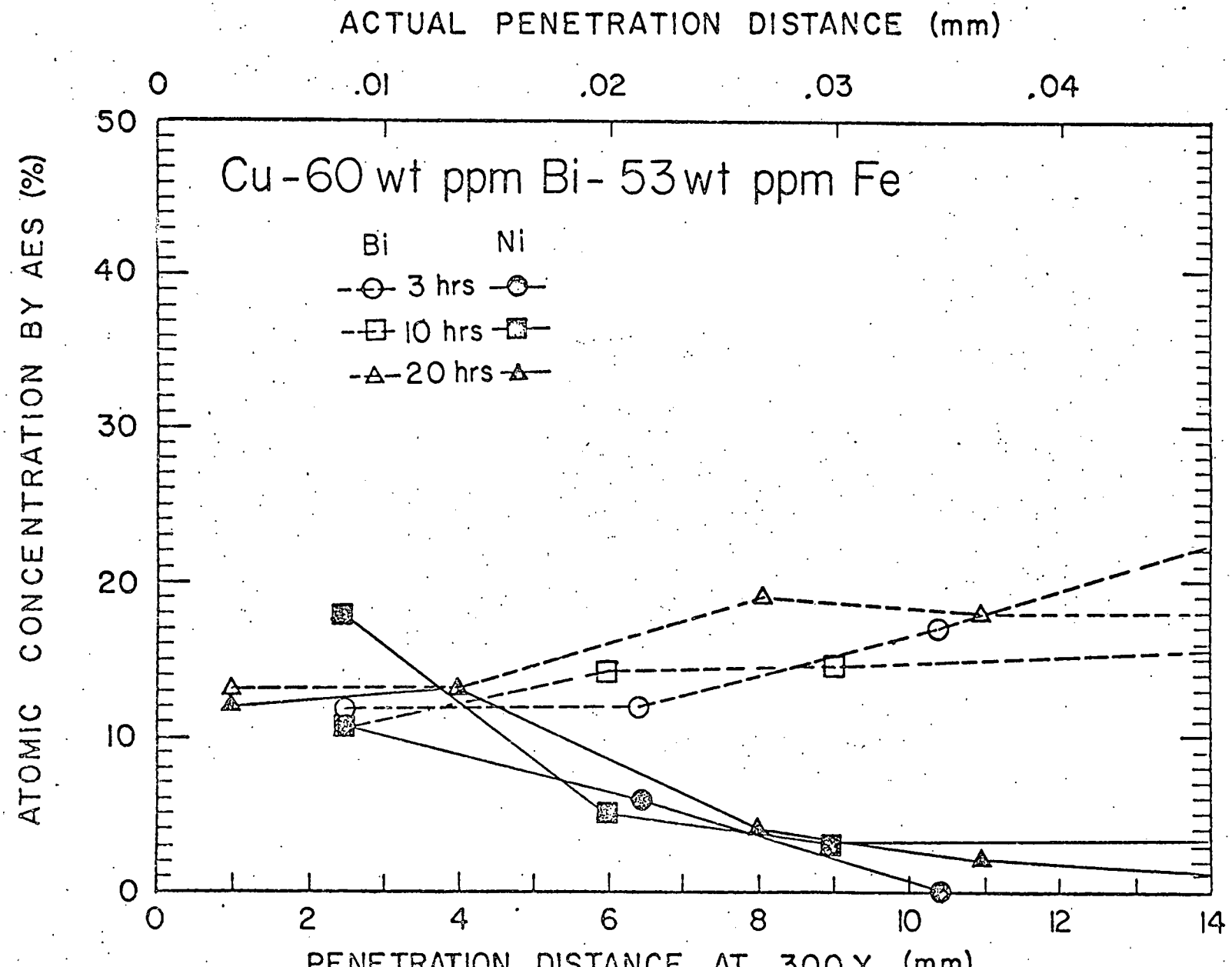

Figure 10. Atomic concentration versus penetration distance, Cu-60 wt ppm Bi-53 wt ppm Fe.

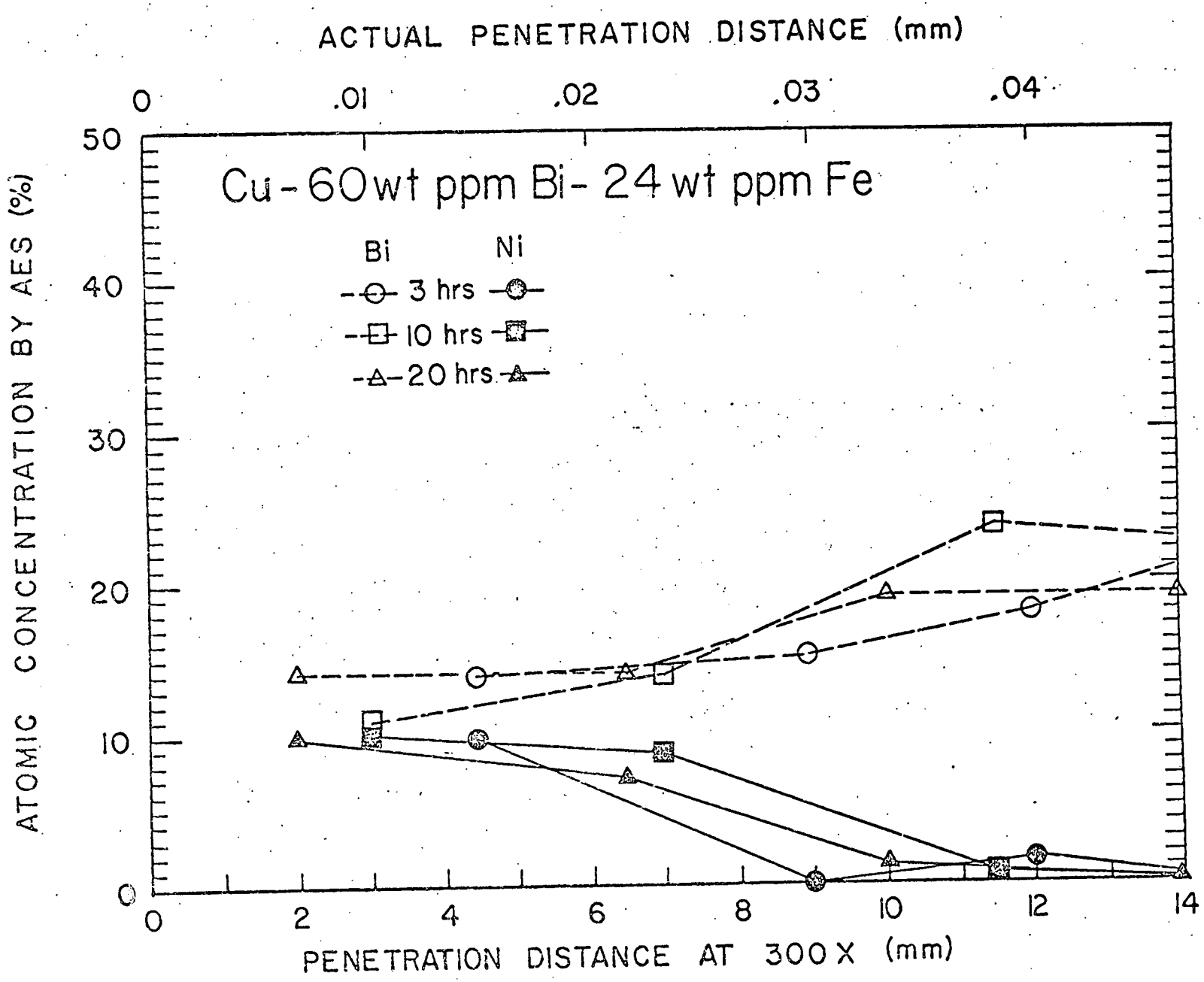

Figure 11. Atomic concentration versus penetration distance, Cu-60 wt ppm Bi-24 wt ppm Fe.

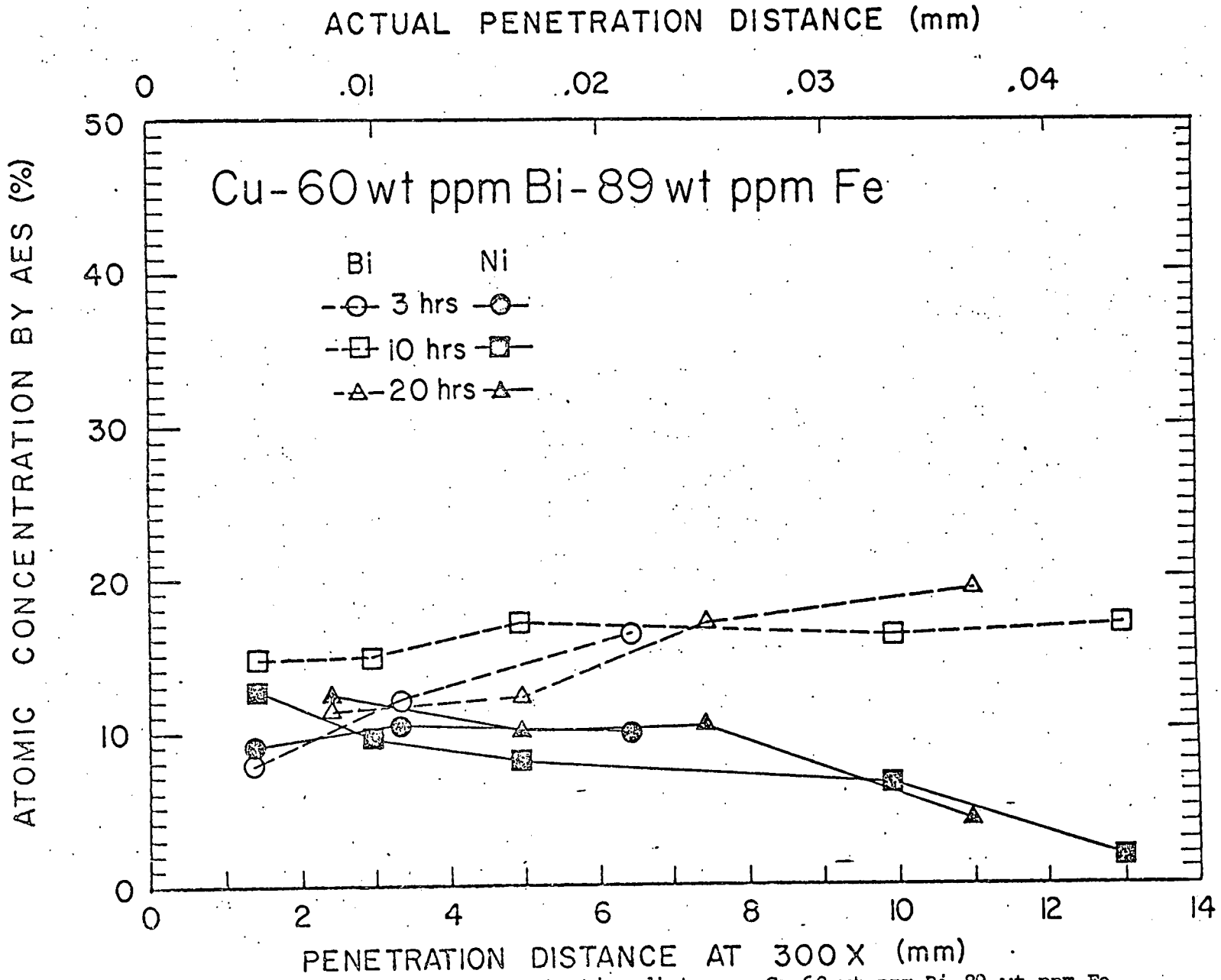

Figure 12. Atomic concentration versus penetration distance, Cu-60 wt ppm Bi-89 wt ppm Fe.

3. The longer the time for diffusion for a given alloy, the more the plateau region extends into the bulk.

4. The Bi concentration and the nickel concentration tend toward a 50/50 ratio.

Item four indicates a positive interaction between Bi and Ni and, upon examination of the Bi-Ni phase diagram, it was found that the phases $NiBi_3$ and NiBi are formed. The heats of formation are not known, but using various thermodynamic arguments, one would estimate a value to be between -400 to -2000 cal/nole. If these estimates are good, one would expect the Ni and Bi to cosegregate to grain boundaries in copper, and they may form a two-dimensional phase. This suggests that the grain boundary diffusion can be retarded effectively by segregating a species that tends to form compounds with the diffusing species. This would be useful where the only consideration is grain boundary diffusion rate, but it probably would render the material grain boundary brittle.

D. Stress Corrosion of Copper Alloys

In previously reported work the susceptibility of admiralty brass (Cu-28Zn-1Sn alloy) to transgranular stress corrosion cracking in acid copper sulfate and copper nitrate environments was described. The dependence of the cracking kinetics upon the solution composition was determined and it was found that crack initiation rates were dependent upon electrolyte composition but crack propagation rates were virtually the same in all solutions causing stress corrosion cracking. It was also shown that the chemical environment within the propagating crack is considerably different than the bulk solution.

A thin tin-rich layer was found on the stress corrosion fracture surface and the source of the tin was proven to be the alloy itself

rather than the chemical environment. It was presumed that processes of solute segregation served to develop a tin-rich path within the admiralty microstructure or else tin dissolved from the alloy was preferentially re-deposited on the fracture surface.

We proposed to determine the role of solute segregation in generating a metallurgical structure susceptible to stress corrosion. For this purpose high purity binary alloys of Cu-Sb, Cu-Bi and Cu-Sn were chosen. Both Sb and Bi were known to segregate intergranularly in copper and both were known to cause intergranular embrittlement. Electrochemical studies of the bulk alloys and of the grain boundary regions were carried out in conjunction with the susceptibility measurements. Both Sb and Bi are more electrochemically active than copper.

1. Stress Corrosion of Cu with Segregated Sb, Bi, or Sn

Dilute sulfuric acid was chosen as an environment for the stress corrosion studies. In order to establish a susceptibility base line, pure Cu was tested. No cracking was observed during tensile testing of the specimens. A noble shift of the corrosion potential was observed. The application of neither anodic nor cathodic potentials served to induce cracking. The results indicate high purity copper has a grain boundary structure and composition that resists attack even when stressed in acid solution.

Cu-Sb alloys containing 0.06, 0.07, 0.24 and 0.31 atom percent (a/o) Sb were prepared. The two most dilute alloys were not embrittled by heat treatments of 525°C and it was concluded that any Sb segregation in these alloys was insufficient to cause intergranular embrittlement in the absence of a corrosive environment. The more concentrated alloys were grain boundary brittle in rapid tensile straining following the segrega-

tion heat treatment. Conversely, grain boundary embrittlement of these alloys was removed by a solutionizing annealing treatment at 850°C for two hours followed by a water quench.

The intergranular fracture surfaces of the two most concentrated Cu-Sb alloys were characterized with respect to fractography and chemical composition. A number of small isolated second phase particles were observed on the fracture surface but not in the bulk alloy. It was concluded that the second phase was a discontinuous grain boundary precipitate. Auger analysis of these fracture surfaces indicates the boundary concentrations of Sb were both about 10 a/o. This common value suggested a definite grain boundary solubility limit. To test this premise, segregation times for both alloys were varied between 3 and 10 hours. For all samples the values were near 10 a/o; all were within the range of 9-12 a/o. To ensure the detected Sb was present mainly as a thin layer of segregant, scanning Auger microscopy was employed to determine the Sb distribution; it was evident that Sb coverage of the intergranular facets was continuous.

Thus an apparent grain boundary solubility limit of 10 a/o exists at 525°C, the limit probably imposed by the formation of the small grain boundary precipitates. A large solute excess (about 90 a/o) predicted for equilibrium grain boundary segregation of Sb in Cu by the McLean expression is not attained at this temperature.

All alloys given the solutionizing heat treatment were immune to stress corrosion in dilute sulfuric acid during static three point bending tests. Following segregation heat treatment the alloy containing 0.24 a/o Sb was clearly susceptible to intergranular stress corrosion. The more dilute alloys were immune to attack while the 0.31 a/o Sb material was attacked by grain boundary and general corrosion -- and not by

stress corrosion cracking. The stress corrosion of the 0.24 a/o material was studied in some detail. Nearly every grain boundary was attacked by the environment, suggestive of grain boundary corrosion; but it was found that in the absence of stress, little general attack and no grain boundary cracking occurred. Stress corrosion crack walls were free of deposits and characterized by bright intergranular facets, which persisted to the crack tip.

For the Cu-Bi studies an alloy containing 180 ppm of Bi was employed. In a correlative study, it was determined that boundary concentrations of 40-90 atom percent of Bi developed during segregation heat treatments. It is noted these concentrations are considerably higher than those measured for Cu-Sb. In three point bending tests in dilute sulfuric acid, segregated samples (heat treated at 525°C) were susceptible to stress corrosion. The attack was similar to that observed for the Cu-Sb alloys. And, again, solutionizing annealing treatments rendered the material immune to stress corrosion. Unstressed bar specimens were similarly immune.

A Cu-Sn alloy containing 0.54% of Sn was prepared and subjected to the three point bending stress corrosion test. Stress corrosion was not observed. Instead the material was attacked by pitting.

2. Electrochemical Studies

The corrosion potentials of the above alloys were measured in 0.2M sulfuric acid. The experimental arrangement is shown in Figure 13. The corrosion potential was not affected by segregation or solutionizing heat treatments; all alloys exhibited corrosion potentials characteristic of the solvent element, copper.

The intergranular embrittlement induced by segregation afforded the unusual opportunity of studying directly the electrochemical properties

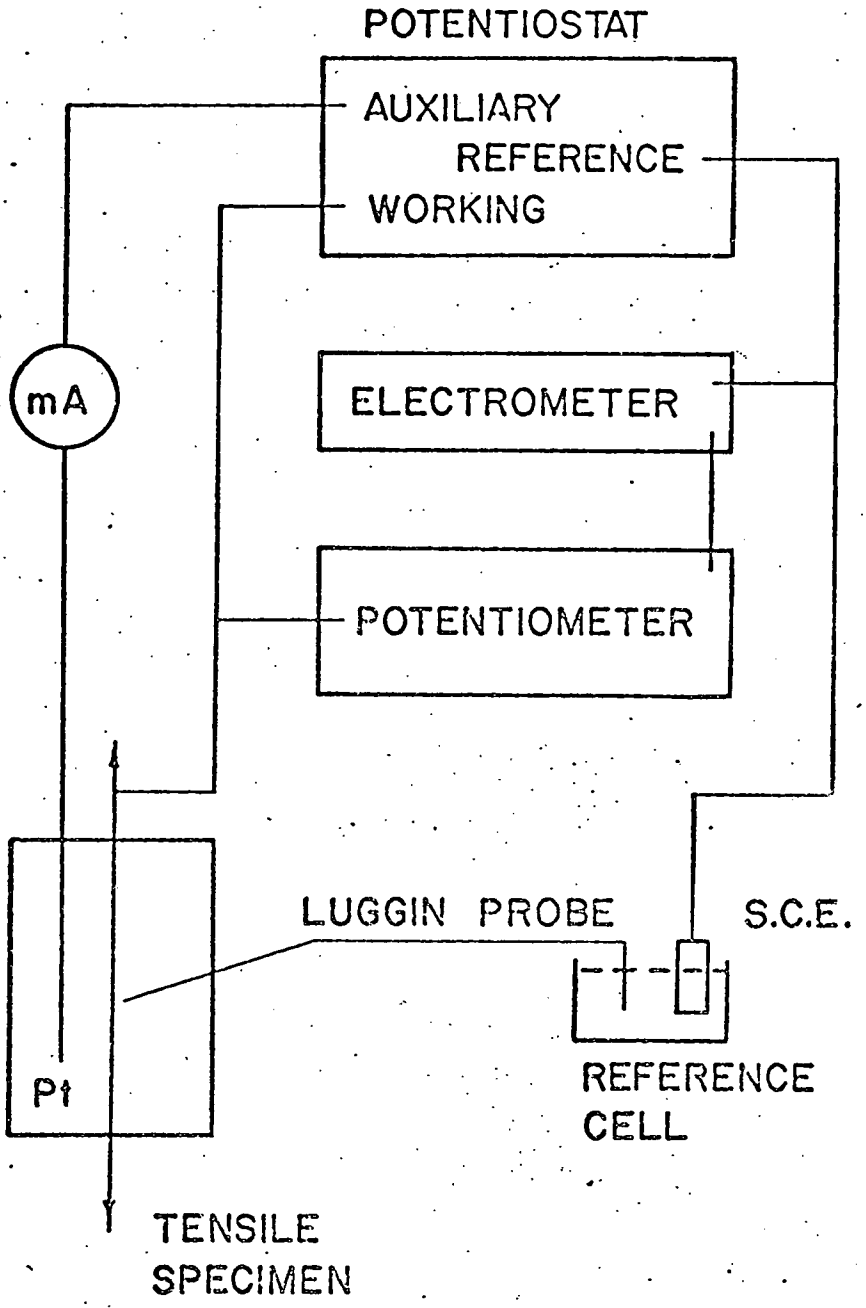

Figure 13. Tension test stress corrosion cell.

of the segregant-rich grain boundary material. Corrosion potential measurements made on intergranular fracture surfaces gave reproducible values that were active with respect to those measured on the bulk alloy surfaces. For the two most concentrated Sb alloys the fracture surface was about 25 mV active with respect to the bulk alloy and was more noble than the corrosion potential of pure Sb. The magnitude of the fracture surface corrosion potential is thus consistent with the Auger measurements, which indicated a definite concentration limit (approximately 10 a/o) for Sb-segregated grain boundaries in Cu. The boundary potential is taken to be a mixed corrosion potential, controlled by the dissolution of both Cu and Sb.

To confirm that the measured potentials were characteristic of the segregated grain boundary, corrosion potential measurements were made on ductile fracture surfaces of pure Cu and solutionized Cu-Sb alloys. The measured potentials were the same as those for the bulk alloy exterior surface. The fracture surface potential measurements accordingly provide direct evidence for the existence of an active electrochemical path at a segregated boundary in these materials. This is taken to be a driving force for the stress corrosion process. The crack morphology and measured crack velocities described above are also consistent with anodic dissolution along the segregated boundaries playing a major role in crack propagation.

The time dependence of the fracture surface corrosion potential also reflected the nature of the segregated boundary in Cu-Sb. A noble shift from the initial active potential occurred, as shown in Figure 14. The final potential established on the fracture surface was the same as for the bulk alloy. Results for both Cu-Sb alloys were the same and the

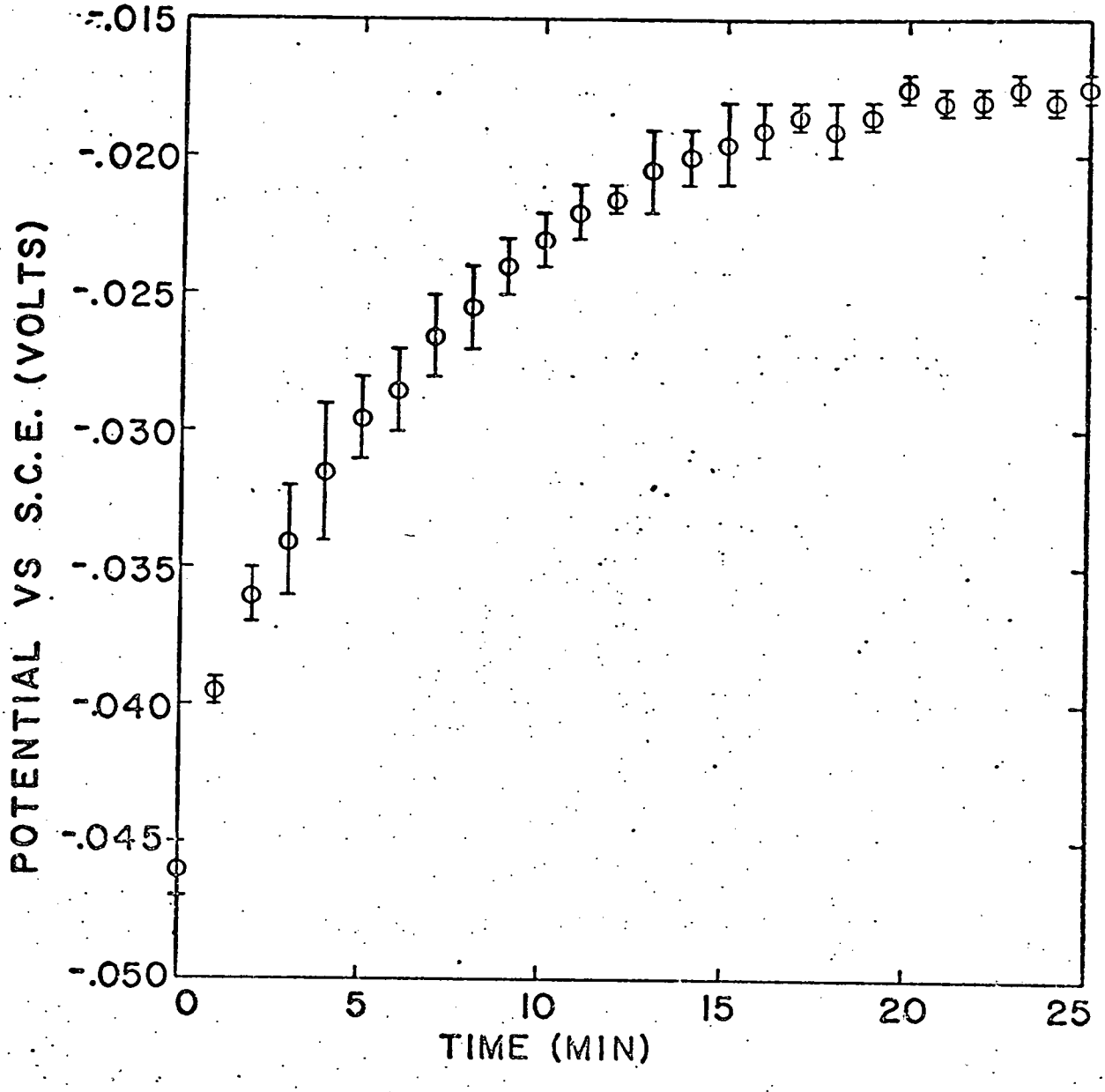

Figure 14. Time dependence of the fracture surface corrosion potential for segregated Cu-Sb 1360.

potential time relation was very reproducible. This noble shift is considered to be the consequence of the removal of Sb segregant from the fracture surface as corrosion proceeded.

Corrosion potential measurements on grain boundary fractures of the segregated Cu-Bi alloy gave somewhat different results. The grain boundary potential was essentailly the same as the corrosion potential for pure Bi; however, the results were not as consistent as those for Cu-Sb. Again, a noble shift, more rapid in this case, occurred with continued exposure to the corrosive environment, the final potential being characteristic of the bulk alloy. A possible cause for the inconsistent potential measurements is the known high degree of anisotropy for Bi segregation to grain boundaries in Cu (10). The noble shift, as before, is considered to result from the removal of the Bi solute by dissolution.

An estimate of the quantity of solute removed by dissolution from intergranular fracture surfaces during the noble shift was made by means of Faraday's Law. The calculated quantity of solute dissolved was equivalent to the removal of about 60 atom layers for Cu-Bi and about 650 layers for Cu-Sb. These calculations confirm that the material affected by the segregant is extremely thin. The values for the Bi rich layer are comparable to sputter profiles measured by Joshi and Stein (11) (about 10 atom layers). The 650 atom layer result for Cu-Sb is considerably greater than that determined by ion sputtering (10-40 atom layers).

3. Conclusions

1) Grain boundary segregation of Sb and Bi in Cu induce stress corrosion susceptibility in sulfuric acid.

2) Electrochemical measurements revealed an active path for stress corrosion.

3) Grain boundary segregation does not affect the bulk electrochemical properties of the unstressed alloys.

III. PUBLICATIONS AND PRESENTATIONS ASSOCIATED WITH CONTRACT

A. Publications

1. Reversible Temper Embrittlement, D. F. Stein, Annual Review of Materials Science, 1, 1977.

2. On the Upper Limit to Equilibrium Segregation at a Grain Boundary, C. L. White and D. F. Stein, Scripta Met., 11, p. 613, 1977.

3. Stress Corrosion Cracking of Admiralty Brass in Aqueous Copper Sulfate, T. R. Pinchback, S. P. Clough and L. A. Heldt, Corrosion, Vol. 32, December 1976.

B. Accepted for Publication

1. Grain Boundary Segregation and Materials Properties by D. F. Stein and L. A. Heldt, to be published in Grain Boundary Segregation, American Society for Metals.

2. A Study of Intergranular Fracture of Cu-Sb Alloys Exposed to Acid Sulfate Solution by T. R. Pinchback and L. A. Heldt, to be published in Environment-Sensitive Fracture of Engineering Materials, The Metallurgical Society, AIME.

3. Sulfur Segregation to Grain Boundaries in Ni_3Al and $Ni_3(Al,Ti)$ Alloys, C. L. White and D. F. Stein, accepted for publication in Met. Trans.

4. Brittle Fracture in Iridium, S. S. Hecker, D. L. Rohr, and D. F. Stein, accepted for publication in Met. Trans.

C. Prepared for Publication

1. Grain Boundary Segregation of Sulfur in Molybdenum, S. M. Tuominen and S. P. Clough.

2. Brittle Grain Boundary Fracture: A Dislocation Dynamics Approach, J. E. Hack and D. F. Stein.

D. Theses Prepared

Master of Science in Metallurgical Engineering

Brittle Grain Boundary Fracture: A Dislocation Dynamics Approach, J. E. Hack.

The Effect of Segregation and Grain Size on the Fracture Strength of Dilute Cu-Bi Alloys, S. J. Vonk.

Doctor of Philosophy in Metallurgical Engineering

The Effect of Bismuth Segregation on the Grain Boundary Diffusion of Ni in Cu, S. P. Clough.

Interfacial Reactivity and Stress Corrosion Cracking of Some Copper Alloys in Acidic Environments, T. R. Pinchback.